Surface-enhanced localized surface plasmon resonance biosensing of avian influenza DNA hybridization using subwavelength metallic nanoarrays

Shin Ae Kim[1]**, Kyung Min Byun**[2,7]**, Kyujung Kim**[3]**,**
Sung Min Jang[1]**, Kyungjae Ma**[4]**, Youngjin Oh**[4]**, Donghyun Kim**[3,4]**,**
Sung Guk Kim[5]**, Michael L Shuler**[6] **and Sung June Kim**[1]

[1] School of Electrical Engineering and Computer Science, Seoul National University, Seoul 151-742, Korea
[2] Department of Biomedical Engineering, Kyung Hee University, Yongin 446-701, Korea
[3] Program of Nanomedical Science and Technology, Yonsei University, Seoul 120-749, Korea
[4] School of Electrical and Electronic Engineering, Yonsei University, Seoul 120-749, Korea
[5] College of Veterinary Medicine, Cornell University, Ithaca, New York 14853, USA
[6] Department of Biomedical Engineering, Cornell University, Ithaca, New York 14853, USA

E-mail: kmbyun@khu.ac.kr

Abstract
We demonstrated enhanced localized surface plasmon resonance (SPR) biosensing based on subwavelength gold nanoarrays built on a thin gold film. Arrays of nanogratings (1D) and nanoholes (2D) with a period of 200 nm were fabricated by electron-beam lithography and used for the detection of avian influenza DNA hybridization. Experimental results showed that both nanoarrays provided significant sensitivity improvement and, especially, 1D nanogratings exhibited higher SPR signal amplification compared with 2D nanohole arrays. The sensitivity enhancement is associated with changes in surface-limited reaction area and strong interactions between bound molecules and localized plasmon fields. Our approach is expected to improve both the sensitivity and sensing resolution and can be applicable to label-free detection of DNA without amplification by polymerase chain reaction.

(Some figures in this article are in colour only in the electronic version)

1. Introduction

Over the past decades, the surface plasmon resonance (SPR) biosensor has been widely used to detect biological interactions including antigen–antibody, protein–protein and DNA–DNA bindings because of its intrinsic advantages such as rapid, quantitative and label-free detection [1, 2]. In principle, SPR is caused by the resonant coupling between incident TM-polarized light and evanescent electromagnetic waves on a metal surface [3]. Since the resonance condition is sensitive to a refractive index change of dielectric environments in the vicinity of a metal film, the SPR technique has been employed to sense the signals originated from biomolecular interactions. However, despite a lot of efforts on improvement of coupling efficiency between biomolecules, it has been difficult to measure a resonance shift at very low concentrations, implying that a thin-film-based SPR biosensor has critical limitations on sensitivity [4].

With the rapid development of nanotechnologies that allows metallic nanostructures to be fabricated and synthesized on the nanometer scale, many interesting approaches for enhanced sensitivity have been introduced [4–7]. It has been empirically shown that the use of metallic

nanostructures enables an efficient optical coupling of incident light to plasmon resonance, so-called localized surface plasmons (LSPs), which have been utilized to amplify the optical signals of the conventional SPR biosensor. This sensitivity improvement is attributed to strong interactions between LSPs and propagating surface plasmons in the presence of nanostructures, resulting in complex resonance properties with an additional shift of resonance angle. In particular, the exploitation of periodic nanostructures can offer the advantages of spatial uniformity and performance reproducibility, while preserving the advantage of label-free SPR detection [8].

As an example of LSP resonance (LSPR) optical sensing, we considered one-dimensional (1D) subwavelength gold nanogratings on a thin gold film [9, 10]. The numerical results have shown that the optimized design of gold nanogratings provides a notable enhancement of sensitivity by more than ten times, compared with conventional SPR biosensors. Also, we experimentally observed 2.42-fold signal amplification in detecting a self-assembled monolayer (SAM) for gold nanogratings of $\Lambda = 200$ nm.

Since the discovery of extraordinary transmission through periodic nanohole arrays [11], researchers have been exploring its applications in LSPR sensing as an alternative to the total internal reflection (TIR) mode based on the Kretschmann configuration, with a particular emphasis on the possibility of multiplexed sensing elements [12–14]. The optical coupling between two-dimensional (2D) nanohole arrays and absorbed molecules has been observed as a noticeable transmission resonance change. Although initial investigations of 2D nanohole arrays have presented poor sensitivity, which is an order of magnitude lower than the results obtained from conventional SPR biosensors [15], recent innovations have allowed for significant improvement in both the sensitivity and measurable detection limits [16–18]. Another peculiar interest of 2D nanohole arrays is polarization dependence [19]. When nanohole arrays with unsymmetrical periodicity are used, different optical transmission resonances are probed according to the incidence polarization. This polarization-dependent biaxial sensing can be used to extend the dynamic range of refractive index detection from a single-nanohole array structure.

However, unlike massive experimental studies on LSPR sensing applications via transmission-type 2D nanohole arrays, where the polarized light is incident from a broadband source and the transmission spectrum is measured, no experimental results using TIR-based reflection-type LSPR detection have been reported combined with 2D nanohole arrays. Considering the potential of developing in-field SPR biosensors with an enhanced sensor performance in a reproducible way, an approach based on a reflection-type SPR configuration is practically appropriate due to its larger sensing length and the accompanying higher sensitivity than for the transmission-type one. Thus, in this context, we intend to demonstrate experimentally that periodic 2D gold nanohole arrays built on a thin gold film can enhance the sensitivity of conventional thin-film-based SPR detection. Note that, since the resonance of a reflection-type LSPR structure occurs only for TM polarization, 2D nanohole arrays with a symmetrical

Table 1. Geometric parameters of three kinds of SPR samples. The symbols of Λ, W, D, d_f and d_g indicate the period of nanostructures, width of 1D nanogratings, diameter of 2D nanohole arrays, and thicknesses of a thin gold film and gold nanostructure, respectively.

Type	Λ (nm)	W or D (nm)	d_f (nm)	d_g (nm)
A Flat gold	—	—	40	—
B 1D nanograting	200	100	40	20
C 2D nanohole	200	80	40	15

period of $\Lambda = 200$ nm are fabricated. In addition, to contrast the influence of nanostructure geometry on sensitivity enhancement, 1D gold nanogratings with $\Lambda = 200$ nm are investigated simultaneously.

In terms of sensing applications, we extend the scope of 1D and 2D nanostructure-amplified SPR to analyzing avian influenza (AI)-DNA hybridization, which is more practical than measuring bulk refractive index changes or SAM formation. Recently, since highly pathogenic AI viruses such as H5N1 and H7N7 have provoked a fatal disease in humans and substantial economic losses due to infection of commercial poultry, rapid and sensitive detection techniques are highly required [20, 21]. Herein, as a preliminary SPR study for the diagnosis of viral diseases, a sectional DNA sequence of AI virus is utilized as a target probe. AI-DNA hybridization experiments indicate that the sensitivity of 1D nanogratings is higher than that of 2D nanohole arrays and that both the surface reaction area and the position of the bound target play an important role in achieving significant SPR amplification.

2. Methods and materials

2.1. LSPR sensor chip fabrication

We fabricated three kinds of working samples: one planar gold film (sample A) and two nanostructure-based LSPR substrates with 1D nanogratings and 2D nanohole arrays (samples B and C), as illustrated in figure 1(a). A gold film with a thickness d_f was first sputtered onto a 20 mm × 20 mm × 1 mm thick SF10 glass substrate after evaporation of 2 nm thick chromium as an adhesion layer. To implement periodic gold nanostructures, 1D or 2D patterns were defined by electron-beam lithography on a PMMA photoresistive layer, followed by sputtering of gold. The nanosized pattern was transferred to form a metallic 1D or 2D nanostructure with a thickness of d_g by lift-off. Subsequently, the gold substrate was cleaned in acetone and 70% ethanol solution for 10 min in a sonication bath. The chip was then rinsed with deionized distilled water (DDW) and finally irradiated by UV light to remove organic residues. Figure 1(b) shows scanning electron microscope (SEM) images of samples B and C. The design parameters of three working samples are listed in table 1.

2.2. Optical measurement set-up

The plasmonic sensor substrates were loaded into a custom-made SPR system to monitor the hybridization reaction in real-time. Incident light from an He–Ne laser ($\lambda = 633$ nm, 25-LHP-991, Melles-Griot, Carlsbad, CA) was passed through a polarizer to produce a TM-mode signal, as presented in figure 2. An optical chopper and lock-in amplifier (SR830
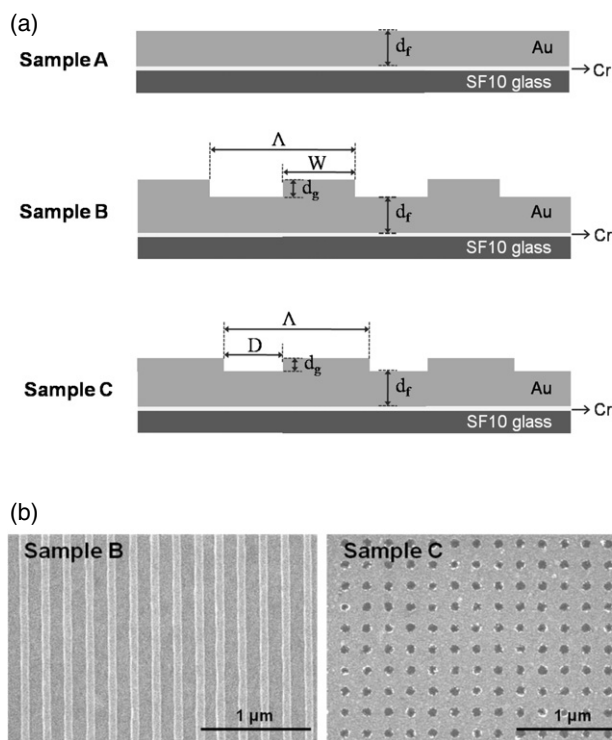
Figure 1. (a) Schematic diagram of three working SPR samples: one thin-film-based SPR sample (sample A) and two nanostructure-based LSPR samples (samples B and C). (b) Scanning electron microscope images of the fabricated LSPR sensor chips of samples B and C.

Figure 2. Schematic diagram of the angle-scanning-type SPR measurement system.

DSP, Stanford Research Systems, Sunnyvale, CA) were employed to reduce the overall noise level. Reflected light from gold substrates was calibrated by a photodiode (818-UV, Newport, Irvine, CA) as an optical detector. Our SPR set-up was based on dual concentric motorized rotation stages (URS75PP, Newport, Irvine, CA) for angle-scanning measurement with a nominal angular resolution of 0.002°. During the AI-DNA hybridization experiments, SPR curves were measured with a resolution of 0.01°. The minimum detectable refractive index of the set-up was estimated to be $\Delta n \sim 1 \times 10^{-6}$ without enhancement [10].

2.3. AI-DNA hybridization protocols

We used HPLC-purified capture oligonucleotide and its complementary target oligonucleotide purchased from Genotech Inc. (Taejeon, Korea). As drawn in figure 3, the base sequences were 5′-Thiol-TTT TTT TTT TTT TTT ATT GGA CAC GAG ACG CAA TG-3′ for capture probes and 5′-CAT TGC GTC TCG TGT CCA AT-3′ for target probes obtained from a partial sequence of avian influenza A virus (A/avian/NY/73-63-6/00(H7N2)) hemagglutinin, which is highly associated with the pathogenicity of AI viruses. The thiol-modified capture probe with 15-thymine spacer was attached to a gold surface to improve hybridization efficiency and a gold–sulfur (from thiol) covalent linkage was constructed. An immobilization buffer of 1 M KH₂PO₄ and hybridization buffer of 1 M NaCl, 10 mM Tris-buffer, pH 7.4, and 1 mM EDTA were used. Dithiothreitol, ethyl acetate and 16-mercaptohexadecanoic acid (MCH) were purchased from Sigma-Aldrich (Saint Louis, MO, USA).

Dithiothreitol and ethyl acetate were used to make a covalent linkage from the thiol-labeled capture probe. All stock oligonucleotide solutions were stored at -20 °C and made with DDW. To detect AI-DNA hybridization, the capture DNA was first immobilized on the SPR sensor substrates. Since thiolated capture probes alone cannot form a uniform coverage, MCH SAM was used to improve hybridization efficiency and displace nonspecific interactions [22]. After the sensor chip was soaked in DDW and the SPR response became stable, 1 μM target AI-DNA was injected and SPR characteristics were monitored until no SPR angle change was observed.

3. Results and discussion

Figure 4(a) shows SPR curves for the three types of gold substrates. The solid and dashed lines indicate the curves before and after the injection of target probes mixed with hybridization buffer. Although the refractive index change induced by 20-mer oligonucleotide interactions without any bound tag was quite small, a distinct variation in SPR responses was clearly observed during the hybridization. The results demonstrate that a larger SPR angle shift occurs for samples B and C, compared with a conventional planar substrate of sample A. Stated another way, significantly enhanced detection of AI-DNA hybridization can be accomplished when using nanostructure-based LSPR biosensors.

To show the consistency of our SPR experiments, AI-DNA interactions were repeatedly measured under identical conditions of a total volume of 100 μl of hybridization solution containing hybridization buffer and 1 μM target probes. Figure 4(b) shows the experimental data of mean values and standard error bars determined by reiterating the hybridization experiments. The resonance angle shifts were 0.080° $\pm$ 0.026° for sample A, 0.324° $\pm$ 0.073° for sample B and 0.203° $\pm$ 0.049° for sample C, respectively. A *p* value smaller than 0.05 for nanostructure-based gold substrates proves the reproducibility of our experiments, where the *p* value denotes the probability of error that is involved in accepting our observed result as valid, that is, as representative of the population. In other words, the higher the *p* value, the less we can believe that the observed relation between variables in the sample is a reliable indicator of the relation between the respective variables in the population. The overall enhancement of the nanostructure-based LSPR biosensor relative to a thin-film-based conventional one was quantitatively evaluated by the sensitivity enhancement factor (SEF), defined as the ratio of resonance angle shift by the target on a nanostructure-based LSPR sample ($\Delta\theta_{\text{LSPR}}$) to that on a flat gold substrate with no nanostructure ($\Delta\theta_{\text{control}}$), i.e. SEF $= \Delta\theta_{\text{LSPR}}/\Delta\theta_{\text{control}}$ [7].
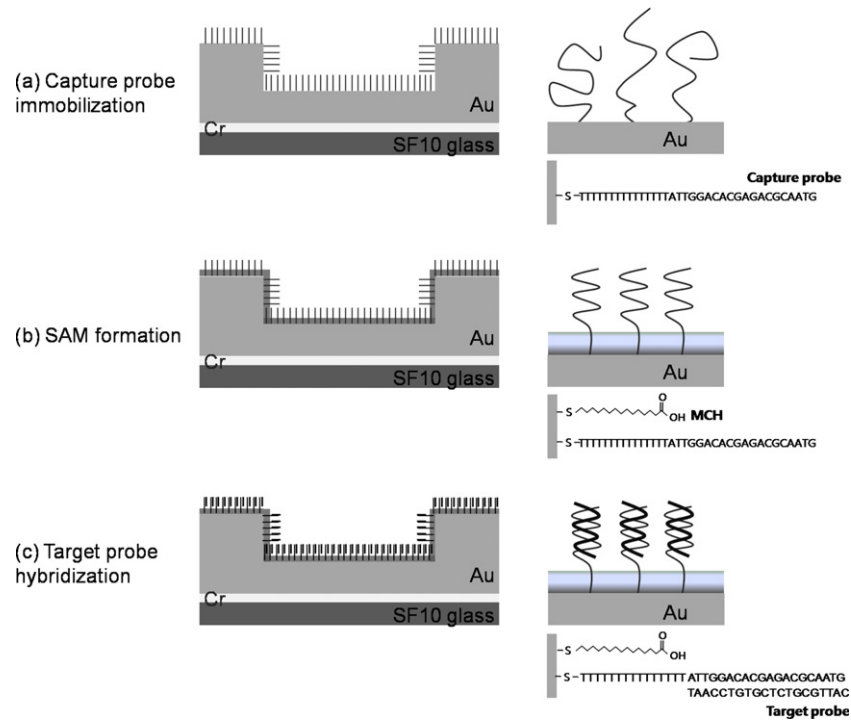
Figure 3. Illustration of capture immobilization, MCH treatment and target AI-DNA hybridization on an LSPR sensor chip.

Table 2. Measured SPR characteristics and SEF and GSAF values.

Type	SPR angle shift		SEF	GSAF
	Average (deg)	Standard error (deg)		
A	0.080	0.0263	1.00	1.00
B	0.324	0.0728	4.05	1.20
C	0.203	0.0491	2.54	1.09

Measured SEF values are listed in table 2. For a fixed period of $\Lambda = 200$ nm, AI-DNA hybridization on sample B produced SEF = 4.05 while SEF = 2.54 for sample C. The larger SEF in sample B is attributed to an increased surface reaction area and strong interactions between biomolecules and locally enhanced plasmon fields. An increment of surface reaction area allows additional interactions between the sensor substrate and adsorbed target analytes. Moreover, from our earlier investigations, it was shown that local field enhancement significantly affects the sensitivity in accordance with the position where the binding events occur [23].

First, in order to quantify the amount of increased surface area, the gross surface area factor (GSAF), the ratio of the total surface reaction area of LSPR substrates (GSA_{LSPR}) to that of a conventional SPR substrate ($GSA_{control}$), was defined as

$$GSAF = \frac{GSA_{LSPR}}{GSA_{control}} = \frac{GSA_{top} + GSA_{bottom} + GSA_{sidewall}}{GSA_{control}}$$
$$= 1 + \frac{GSA_{sidewall}}{GSA_{control}}. \tag{1}$$

The LSPR sensor substrates with 1D or 2D nanostructures can be divided into three regions: top, bottom, and sidewalls, denoted, respectively, by GSA_{top}, GSA_{bottom} and $GSA_{sidewall}$. $GSA_{control}$ equals the sum of GSA_{top} and GSA_{bottom} and the

GSAF remains constant regardless of the surface dimension if the periodic nanostructures have a high aspect ratio. GSAF per period can substitute for the GSAF value in equation (1). Considering the geometric parameters in table 1, GSAF values were calculated to be 1.20 for sample B and 1.09 for sample C and this may prove a higher SEF for sample B. The strong correlation between the surface-limited increase of reaction area and the enhanced sensitivity was also reported by Oh *et al*, representing notable amplification in the resonance shift by employing mesoporous silica substrates with a high pore volume [24].

Second, it is also important to note that an increase of overall surface reaction area is fully associated with the sidewalls of 1D or 2D gold nanostructures and the relatively small-sized dimension of the sidewalls leads to a significant improvement in sensitivity. In conjunction with [23], we attribute it to the sidewall effect. Especially of interest is that qualitative trends inferred from figure 4 agree well with our previous works on the influence of target localization. It was demonstrated that target analytes on the sidewalls of metallic nanostructures make a significant contribution to sensitivity enhancement due to intensive overlap with multiple localized plasmonic fields, though the overall sensitivity enhancement is determined by the summation of plasmonic interactions on the top, bottom and sidewalls. Namely, molecular interactions occurring at sidewalls take advantage of plasmonic field localization, which can induce extremely large enhancement of sensitivity by more than an order compared to a conventional SPR biosensor. This corresponds well with our experimental results since nanostructure-based LSPR substrates with shallow sidewalls presented notable sensitivity improvement and sample B with a broader sidewall area exhibited a larger SEF than sample C.
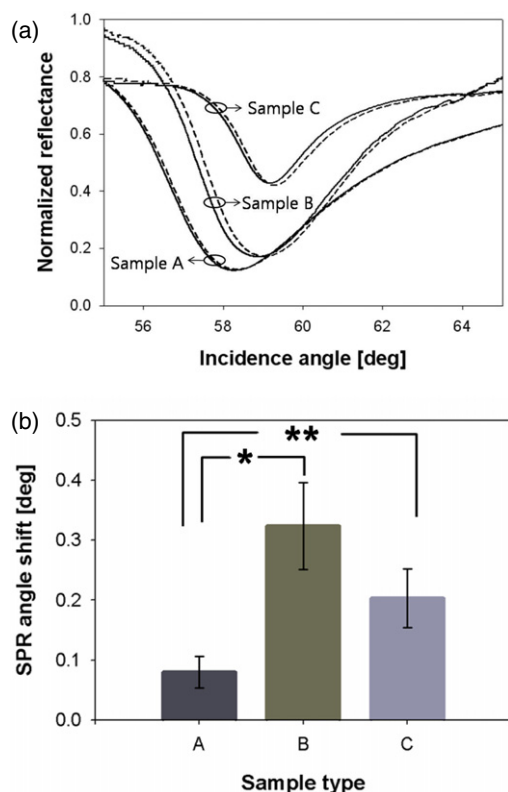
Figure 4. (a) SPR responses of the three working samples for AI-DNA hybridization experiments. The solid and dashed curves represent before and after AI-DNA hybridization, respectively. (b) Statistical data of resonance angle shift after AI-DNA hybridization experiments for sample A (control, $n = 9$), sample B ($n = 5$, $^{*}p < 0.01$ versus control) and sample C ($n = 3$, $^{**}p < 0.05$ versus control).

To confirm the above plasmonic interpretations of sensitivity enhancement, we visualize the electromagnetic fields near the sensor surface by calculating the spatial field distributions based on the finite-difference time-domain (FDTD) method. The minimum grid size is 1 nm and the geometric parameters of sample B for FDTD calculation are described in table 1. The field distribution is obtained when TM-polarized light with a wavelength of 633 nm and an incidence angle of 64.57° illuminates the gold substrates, where DNA hybridization modeled as a 3 nm thick dielectric

monolayer occurs in an aqueous solution. From the field calculation of $|E_X|$ for 1D gold nanogratings, figure 5(a) presents well-known features of hot spots, as LSPs are highly excited at the vertices of rectangular nanogratings and decay rapidly when one moves further away from the surface. On an assumption of light incidence of unit amplitude, a maximum field amplitude of $|E_X|$ was obtained of 12.2. In particular, the field intensity normalized by 3.00 clearly shows the field contrast between sidewalls and other surface areas of 1D nanogratings (see figure 5(b)). In short, enhanced fields occurring at the sidewalls may amplify the optical signals of biointeractions more effectively than those at nanograting tops and bottoms.

While the results are not shown, the field distribution of 2D nanohole arrays also presented enhanced local fields at the nanohole sidewalls. However, due to the prolonged FDTD computation time and the complex field patterns at the sidewalls, an exact plasmonic interpretation of the sidewall effect for 2D nanohole arrays is not possible yet. In the near future, the details will be demonstrated in our subsequent studies after in-depth discussions on the field localization for nanohole arrays and its influence on sensitivity enhancement.

Another interesting topic from the viewpoint of actual biosensing applications is that polymerase chain reaction (PCR)-free DNA detection is highly desired for rapid clinical diagnosis of genetic diseases [25, 26]. Despite its powerful advantages such as high fidelity and unlimited amplification ability, the conventional PCR technique demands complex instruments and time-consuming and troublesome processes. Also, as the PCR method is often liable to contamination, it is not yet appropriate for rapid and *in situ* DNA detection and for point-of-care diagnostics. Accordingly, in order to develop a PCR-free DNA biosensor, the SPR technique has been intensively investigated. Unfortunately, the inability of conventional SPR to measure extremely small changes in refractive index hinders its application in DNA detection at very low concentrations. While the theoretical resolution limit that has been reported of a thin-film-based SPR biosensor with an angular interrogation scheme is as small as 1 pg mm^{-2}, corresponding to a change of 5×10^{-7} in refractive index [1], a typical value of the minimally detectable change in molecular weight is obtained as approximately several tens or hundreds pg mm^{-2} due to an instrumental resolution limit and various noise factors in experiments.
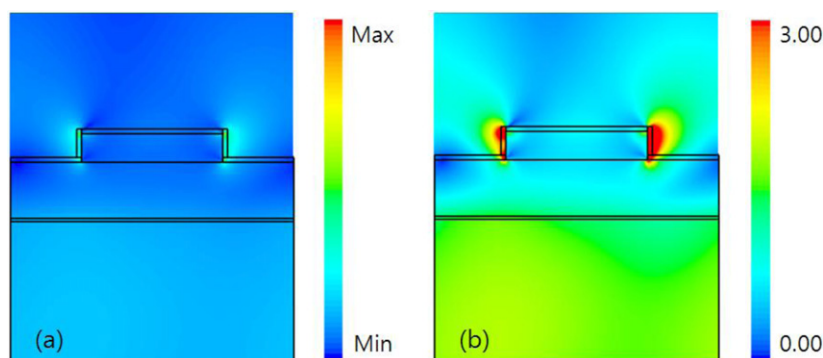
Figure 5. (a) Field profile of $|E_X|$ calculated by the FDTD method for sample B and (b) the one normalized by a value of 3.00.

To address this drawback, an SPR-based DNA detection technique combined with radiolabeling [27], fluorescence [28] and colloidal gold nanoparticles [6] has been introduced. Among them, while the lowest amount of hybridized target DNA was achieved up to 10–20 fmole mm^{-2} and indeed this result demonstrates the possibility of a PCR-free biosensor [29], their substantial interest has been focused on utilizing external labels providing high molecular weight or high refractive index, consequently eliminating the advantage of label-free SPR detection. On the other hand, in this study, LSPR configurations with 1D or 2D metallic subwavelength nanostructures on a gold film can offer the advantages of spatial uniformity and performance reproducibility, while preserving the advantage of label-free detection. Importantly, in terms of sensor resolution which means the minimum change in the parameter to be determined which can be resolved by a sensing device [1], taking account of the 100 μl solution volume and the cylindrical well with a diameter of 9 mm, a target AI-DNA concentration of 1 μM in this study was estimated to match a maximum of 390 fmole mm^{-2} (this value corresponds to 2.4 ng mm^{-2} or 2.36×10^{13} oligonucleotides cm^{-2}) for 20-mer oligonucleotides. Note that this calculation assumes 100% of the oligonucleotides in the target solution hybridized to the sensor surface. It should also be emphasized that, when we consider a maximum resonance shift of 0.324° for sample B and an instrumental angle resolution of 0.01°, the minimum sensor resolution of about 12 fmole mm^{-2} can be realized. This resolution approaches that of radiolabeling methods. Additional improvements in the minimum sensing resolution can be achieved by optimizing hybridization conditions and reducing the background caused by nonspecific interactions [6]. As a result, this study demonstrates the advantage of using periodic metallic nanostructures for SPR signal amplification and opens up the potential of SPR to implement a PCR-free hybridization biosensor and for DNA diagnosis in a reproducible way.

4. Concluding remarks

In this study, a 2D subwavelength gold nanohole array was introduced to improve the sensitivity of a thin-film-based reflection-type SPR biosensor. Its SEF value obtained at $\Lambda = 200$ nm was 2.54 for detecting AI-DNA hybridization, which is attributed to an increased surface reaction area and stronger coupling between target analytes and excited LSPs supported by the nanohole arrays. Moreover, due to the sidewall effects, the SPR signal can be amplified up to four times for 1D gold nanogratings, yielding better sensitivity performance than is the case of 2D gold nanohole arrays. The sensitivity and sensing resolution of LSPR sensors employing 1D and 2D gold nanostructures were evaluated quantitatively and presented a potential for future applications in rapid and ultrasensitive hybridization detection and PCR-free clinical diagnosis of genetic diseases.

Acknowledgments

References

[1] Homola J, Yee S S and Gauglitz G 1999 *Sensors Actuators* B **54** 3–15
[2] Cooper M A 2003 *Anal. Bioanal. Chem.* **337** 834–42
[3] Raether H 1988 *Surface Plasmons on Smooth and Rough Surfaces and on Gratings* (Berlin: Springer)
[4] Hu W P, Chen S-J, Huang K-T, Hsu J H, Chen W Y, Chang G L and Lai K-A 2004 *Biosens. Bioelectron.* **19** 1465–71
[5] Sepúlveda B, Angelomé P C, Lechuga L M and Liz-Marzán L-M 2009 *Nano Today* **4** 244–51
[6] He L, Musick M D, Nicewarner S R, Salinas F G, Benkovic S J, Natan M J and Keating C D 2000 *J. Am. Chem. Soc.* **122** 9071–7
[7] Byun K M, Yoon S J, Kim D and Kim S J 2007 *Opt. Lett.* **32** 1902–4
[8] Malic L, Cui B, Veres T and Tabrizian M 2007 *Opt. Lett.* **32** 3092–4
[9] Byun K M, Kim S J and Kim D 2005 *Opt. Express* **13** 3737–42
[10] Kim K, Kim D J, Moon S, Kim D and Byun K M 2009 *Nanotechnology* **20** 315501
[11] Ebbesen T W, Lezec H J, Ghaemi H F, Thio T and Wolff P A 1998 *Nature* **391** 667–9
[12] Tetz K A, Pang L and Fainman Y 2006 *Opt. Lett.* **31** 1528–30
[13] Stewart M E, Mack N H, Malyarchuk V, Soares J A N T, Lee T-W, Gray S K, Nuzzo R G and Rogers J A 2006 *Proc. Natl Acad. Sci. USA* **103** 17143–8
[14] De Leebeeck A, Kumar L K S, de Lange V, Sinton D, Gordon R and Brolo A G 2007 *Anal. Chem.* **79** 4094–100
[15] Brolo A G, Gordon R, Leathem B and Kavanagh K L 2004 *Langmuir* **20** 4813–5
[16] Pang L, Hwang G M, Slutsky B and Fainman Y 2007 *Appl. Phys. Lett.* **91** 123112
[17] Chen H M, Pang L, Kher A and Fainman Y 2009 *Appl. Phys. Lett.* **94** 073117
[18] Lesuffleur A, Im H, Lindquist N C and Oh S-H 2007 *Appl. Phys. Lett.* **90** 243110
[19] Eftekhari F, Gordon R, Ferreira J, Brolo A G and Sinton D 2008 *Appl. Phys. Lett.* **92** 253103
[20] Takemoto D K, Skehel J J and Wiley D C 1996 *Virology* **217** 452–8
[21] Xu J, Suarez D and Gottfried D S 2007 *Anal. Bioanal. Chem.* **389** 1193–9
[22] Steel A B, Herne T M and Tarlov M J 1998 *Anal. Chem.* **70** 4670–7
[23] Byun K M, Jang S M, Kim S J and Kim D 2009 *J. Opt. Soc. Am.* A **26** 1027–34
[24] Oh S, Moon J, Kang T, Hong S and Yi J 2006 *Sensors Actuators* B **114** 1096–9
[25] Teles F R R and Fonseca L P 2008 *Talanta* **77** 606–23
[26] Junhui Z, Hong C and Ruifu Y 1997 *Biotechnol. Adv.* **15** 43–58
[27] Schwarz T, Yeung D, Hawkins E, Heaney P and McDougall A 1991 *Trends Biotechnol.* **9** 339–40
[28] Duggan D J, Bittner M, Chen Y, Meltzer P and Trent J M 1999 *Nat. Genet. Suppl.* **21** 10–5
[29] Watts H J, Yeung D and Parkes H 1995 *Anal. Chem.* **67** 4283–9